DOI 10.24425/aee.2024.148853

Small-signal transmittances of the non-ideal flyback switch-mode DC–DC converter

MACIEJ BĄCZEK, WŁODZIMIERZ JANKE, JAROSŁAW KRAŚNIEWSKI ✉

Department of Electronics and Computer Science, Koszalin University of Technology
2 Śniadeckich Street, 75-453 Koszalin, Poland
e-mail: {maciej.baczek/wlodzimierz.janke/ ✉ jaroslaw.krasniewski}@tu.koszalin.pl

(Received: 04.07.2023, revised: 01.02.2024)

Abstract: Small-signal transmittances of the power stage of a flyback converter in continuous conduction mode are derived on the averaged model obtained by the separation of variables approach. The precise knowledge of these transmittances is necessary in the design process of the converter control circuit. Apart from mathematical formulas for transmittances, the numerical calculations of the frequency dependencies of the transmittances for the assumed set of the converter parameters are presented with the parasitic resistances of components taken into account. The results of the calculations are compared with the measurements performed on the laboratory model of the converter and a good consistency is observed. It is concluded, that the results of the paper may be useful in the designing process of a control circuit of the flyback converter.

Key words: continuous conduction mode (CCM), DC–DC converters, flyback, small-signal transmittances

1. Introduction

Switch-mode DC–DC converters find a great amount of applications and are steadily developed [1, 2]. Transformer-based converters are an important group and have unique features, in particular, the galvanic isolation between input and output, broad range of the voltage transfer functions, the possibility to generate multiple outputs. The most representative example of the transformer-based converters is a flyback converter. Many aspects of a flyback behavior, applications, control and modifications are presented in the literature. References [3–5] may serve as examples. Reference [3] is addressed to the important phenomenon of the parasitic oscillations

occurring at the moments of switching in a flyback converter. The relationship between the occurrence of transformer leakage inductance and the output capacitance of the transistor was identified as the cause of this phenomenon. It was proposed to reduce the ringing losses by using a dissipative RC–RCD clamp. An application solution based on a flyback converter can be found in publication [4]. This paper presents the design of a photovoltaic/battery system using a flyback converter. A dual-output flyback converter is used, enabling DC voltage and high-frequency AC voltage. In the proposed system, the input energy of the PV system is efficiently utilized by using MPPT technique, and the battery charging is controlled by a bidirectional DC–DC converter. The final result is a constant voltage for different loads under varying solar conditions. The cited article [5] discusses a method for designing and modelling an isolated flyback converter based on creating equivalent models for the on and off periods of the switches. The modelling is carried out both with and without parasitic components.

Each switch-mode power converter consists of a power stage and a control circuit. The efficient design of the control circuit is based on the knowledge of the power stage dynamic characteristics. The dynamic behavior of a switch-mode converter may be considered in two-time scales (or two frequency ranges). The fast transients (or the features in the high frequency range) are observed in the single switching period T_S, where the results of the parasitic capacitances of switches and leakage inductances of the transformer coils are visible in the form of the high frequency oscillations. The low-frequency behavior, for frequencies much smaller than the switching frequency, are the results of the external signals, for example, changes of the input voltage or the load current, or may be attributed to the power stage characteristic frequencies, dependent on the product $L \cdot C$, where L and C are the components of the power stage.

The theoretical modeling of switch-mode power converters has been discussed in very large numbers of sources including textbooks, application notes and papers and various approaches to this task may be found. The typical purpose of the power stage modeling is to find the description of its dynamic behavior, to be used in the control stage design. The most convenient form of the power stage dynamics description in a low frequency range is a set of small-signal transmittances [1]. Such transmittances may be considered as a special case of the power stage averaged models and are derived in several steps. First, the large-signal averaged models i.e. nonlinear relations between circuit variables averaged over single switching period are found. In the second step, the small-signal equivalent of the averaged large-signal model is found after representing each circuit variable (and duty ratio of the controlling signal) as a sum of the DC component and small "perturbation" signal. Large-signal and small-signal averaged models may be represented in the form of equivalent circuits. The exact knowledge of the small-signal transmittances of switch-mode converters is necessary to find the proper transmittance of the control circuit and consequently, to assure a good quality of the resulting converter as a closed loop system. The placement of the poles and zeros of the power stage transmittances are especially important in the design procedure.

The averaged models of switch-mode DC–DC converters may be obtained in several ways, which has been well described in the literature. The traditional methods presented among the others in textbooks (for example [1] and [2]) and many papers are based on so called state-space averaging or on switch averaging approach. Another approach to averaged model creation is based on the separation of variables [6, 7]. The averaged models of ideal simple converters working in continuous conduction mode (CCM) obtained by the three mentioned methods are identical. Some differences between the models obtained by different methods are sometimes observed for

discontinuous conduction mode of operations or for non-ideal converters with parasitic resistances taken into account.

The large-signal and small-signal models of transformer-less converters are most frequently presented in the literature. The number of the descriptions of the flyback averaged models is not so high and the examples may be found in papers [8–20].

Some averaged model descriptions of a flyback converter are universal [8–13], and others are addressed to converters with a selected control loop [14–20]. The averaged models of a flyback presented in the literature are usually the models of ideal converters (without parasitic resistances) [9,11,16,18] or converters with parasitic effects only partially included [12–15,17,19]. The complete set of parasitic resistances is included only in the models presented in [8] and [10]. The model descriptions shown in the majority of the above mentioned papers are not verified experimentally [8–12,14,15,18]. The partial experimental verifications of the models may be found only in [13,16,17,19].

Universal, small signal models of flyback are discussed in paper [8] and in PhD dissertation [11]. In particular, in paper [8], by the use of the switch averaging approach, the set of small-signal transmittances (input-to-output, control-to-output and input and output impedances for continuous conduction mode) are found in the analytical form and the series of numerical calculations for assumed values of converter parameters are presented. A set of parasitic parameters of transformer, capacitor and semiconductor switches are included in the analysis and calculations. The derivation of small-signal transmittances of flyback in dissertation [11] is based on the state-space averaging approach. Both operation modes of the converter (CCM as well as DCM) are considered, but only an ideal case (without parasitic resistances of components) is assumed. Unfortunately, the analytical description of small-signal transmittances presented in [8] and [11] is not verified experimentally. The small-signal averaged transmittances of the buck-boost converter are discussed in [21]. The results of [21] may be interesting, because the structure of buck-boost converter is similar to that of flyback.

The main purpose of the present paper is to describe the dynamic behavior of the basic variant of a flyback converter in the form of the set of averaged small-signal transmittances with the complete set of the parasitic resistances of the converter components taken into account, and to verify experimentally the theoretical description. The averaged model presented here is obtained with the use of the separation of variables approach.

2. Flyback converter description

The power stage of the flyback converter considered in the paper is shown in Fig. 1. Voltage generator v_G represents the source of power and conductance G – the load. The transistor (typically – MOSFET) is known as a main switch ($S1$) and $S2$ is an auxiliary switch (a diode in an asynchronous converter as shown in Fig. 1 or a second transistor in a synchronous one).

In the analysis, simulation and design of the converter, the proper description in the form of equivalent circuits is used. The examples of such circuits are presented in Fig. 2.

In Fig. 2(a) an ideal equivalent circuit is depicted, in which $S1$ and $S2$ are ideal switches (short circuit in the ON state, open circuit in the OFF state). The transformer is represented by the pair of controlled sources and the magnetizing inductance L. This inductance and capacitor C are lossless

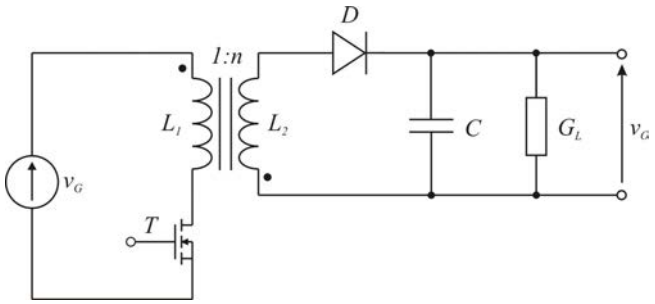

Fig. 1. The power stage of a flyback converter – "v_G – input voltage, v_O – output voltage"

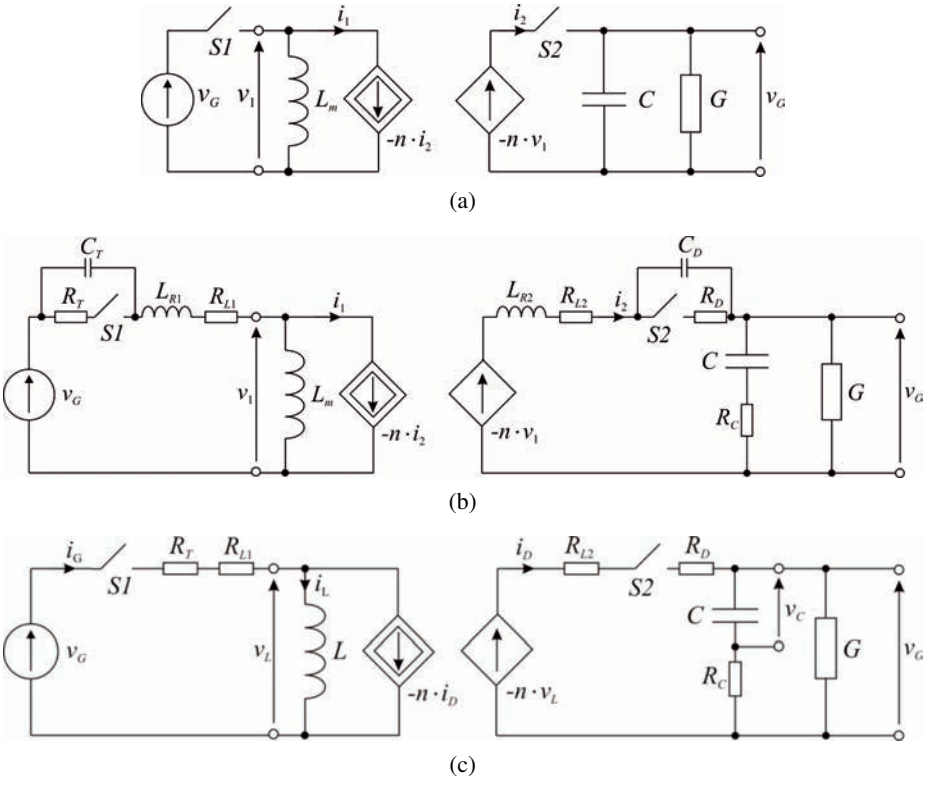

Fig. 2. Equivalent circuits of the power stage of a flyback converter: (a) ideal; (b) with several parasitic components; (c) with the parasitic components important in the low-frequency range

and linear devices. In the non-ideal equivalent circuit shown in Fig. 2(b), the parasitic effects in the converter components are taken into account, in particular, series resistances of components, leakage inductances of the input and output coils of transformer and the output capacitances of switches.

The description of parasitic effects may be modified, for example by introducing parasitic inductance of capacitor, parasitic capacitances of coils and the more involved models of switches (such as models in the SPICE library). On the other hand, in the derivation of averaged models, only the resistive parasitic components are included, (as in Fig. 2(c)), because parasitic inductances and capacitances are negligible in a low-frequency range. The further analysis and calculations are based on equivalent circuit of Fig. 2(c).

Two basic modes of the converter operation are possible – continuous conduction (CCM) and discontinuous conduction (DCM). The boundary between CCM and DCM is sometimes considered and is referred to as a critical conduction mode. The CCM mode is the most frequently used and this mode is considered in the present paper.

3. Theoretical considerations

3.1. Averaged models

Large-signal averaged model of the non-ideal flyback converter in CCM, obtained by the separation of variables has been presented in [22] and [23]. The equivalent circuit representing the large signal model shown in [22] is repeated here for convenience in Fig. 3, together with Eqs. (1)–(3). The small letters with capital letter subscripts used in Fig. 3 as well as in the further text (as for example v_G, i_G, d_A, denote the instantaneous, large signal currents and voltages averaged over a single switching period. The capital letters with the capital letter subscripts (as for example V_G, I_G, D_A), denote the quiescent point terms of the respective quantities.

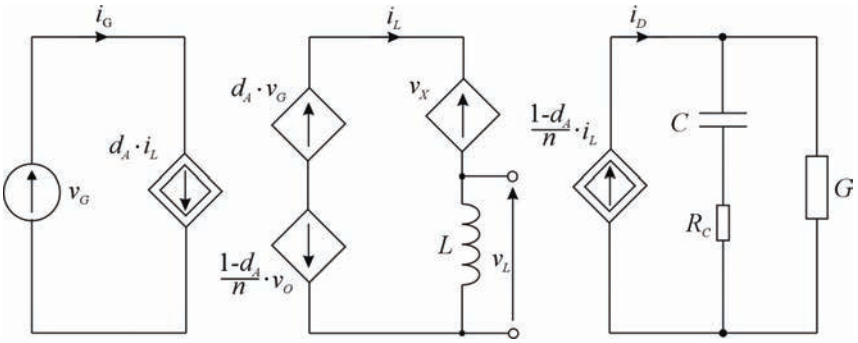

Fig. 3. Large-signal averaged model of a non-ideal flyback converter in CCM [20]

The symbols used in Fig. 3 are explained below.

$$v_X = i_L \cdot \left[d_A \cdot R_{TL} + (1 - d_A) \cdot \frac{R_{DL}}{n^2} \right], \tag{1}$$

$$R_{TL} = R_T + R_{L1}, \tag{2}$$

$$R_{DL} = R_D + R_{L2}. \tag{3}$$

A small-signal averaged model of a flyback converter is obtained from the large-signal model similarly as in the case of simple converters by the proper mathematical operations [1, 2]. The

result for *CCM* is shown in Fig. 4 in the form of the equivalent circuit. Here and in the further considerations, the capital letters with small-letter subscripts denote the small-signal terms of currents and voltages representations in the s-domain. In particular, the s-domain representations of small signal term of circuit variables are denoted as: input and output voltage: V_g and V_o, input current: I_g, the current in magnetizing inductance: I_l, duty ratio: Θ. Current I_o is used only for the definition of the output impedance Z_o. In the definitions of the other transmittances, this current is assumed to be zero.

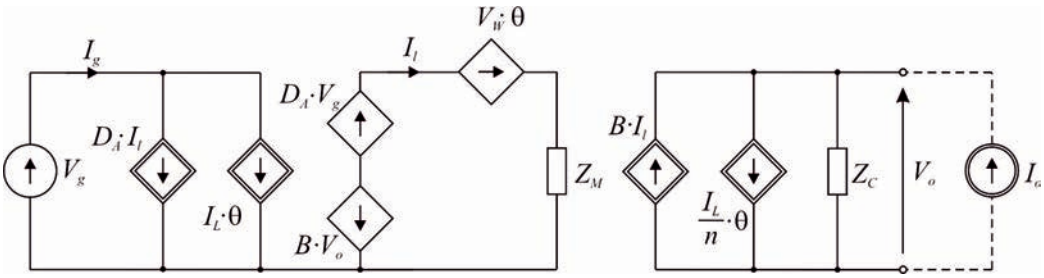

Fig. 4. Small-signal averaged model of a flyback converter in CCM

The above model is then used to the derivation of the small-signal transmittances of the converter. The additional symbols used in Fig. 4 are described as:

$$Z_C = \frac{s \cdot C \cdot R_C + 1}{s \cdot C_Z + G}, \tag{4}$$

$$Z_M = R_M + s \cdot L, \tag{5}$$

$$R_M = D_A \cdot R_{TL} + (1 - D_A) \cdot \frac{R_{DL}}{n^2}, \tag{6}$$

$$B = \frac{(1 - D_A)}{n}, \tag{7}$$

$$C_Z = C \cdot (1 + R_C \cdot G), \tag{8}$$

$$V_W = V_G + \frac{V_O}{n} - R_{XN} \cdot I_L, \tag{9}$$

$$R_{XN} = R_{TL} - \frac{R_{DL}}{n^2}. \tag{10}$$

3.2. Small-signal transmittances

Applying the standard definitions of the input-to-output transmittance H_g, control-to-output transmittance H_d, input admittance Y_{in} and output impedance Z_{out} to the model shown in Fig. 4, one obtains:

$$H_g = \left.\frac{V_o}{V_g}\right|_{\theta=0} = \frac{D_A \cdot B \cdot Z_C}{Z_M + B^2 \cdot Z_C}, \tag{11}$$

$$H_d = \left.\frac{V_o}{\theta}\right|_{V_g=0} = \frac{V_W \cdot B \cdot Z_C - \frac{I_L}{n} \cdot Z_C \cdot Z_M}{Z_M + B^2 \cdot Z_C}, \tag{12}$$

Table 1 continued from previous page

Symbol	Value	Unit
Q	0.414	
$\omega_{Z\,1}$	$2.8 \cdot 10^4$	[rad/s]
$\omega_{Z\,2}$	$-2.611 \cdot 10^5$	[rad/s]
$\omega_{Z\,3}$	$2.027 \cdot 10^4$	[rad/s]
$\omega_{Z\,4}$	691.697	[rad/s]

Table 2. Parameter values of the transfer functions of the ideal converter, calculated from Formulas (30)–(38)

Symbol	Value	Unit
H_{gi} (0)	0.2	[V/V]
H_{di} (0)	16	[V]
$Z_{\mathrm{out}i}(0)$	0	[Ω]
$Y_{\mathrm{in}i}(0)$	0.013	[S]
ω_{0i}	$9.292 \cdot 10^3$	[rad/s]
Q_i	13.102	
$\omega_{Z\,2i}$	$-2.813 \cdot 10^5$	[rad/s]
ω_{Z4i}	691.697	[rad/s]

values. The examples of such comparisons for the output impedance of converter is shown in Figs. 10 and 11. Graphs in Fig. 10 are obtained for several values of parasitic resistances of transistor (R_T) and diode (R_D) assumed to be equal ($R_T = R_D$), with other parasitic resistance values the same as used in calculations presented in Figs. 6–9. According to calculations presented in Fig. 11, the influence of resistances R_T and R_D on the output impedance differs substantially. It may be explained by the form of Eq. (6) for equivalent resistance R_M in which the resistance R_{DL}, dependent mainly on the diode resistance R_D, is divided by n^2. In the converter under considerations, the parameter n equals 0.2 therefore, according to Eqn. (6), the term connected with the resistance R_D is multiplied by 25.

Another comparison is presented in Fig. 12 and concerns the input-to-output transmittance H_g. The curves for the real converter (with parasitic resistances) are compared with curves for the ideal converter (with all parasitic resistances set to zero). The substantial differences are observed, especially in the vicinity of the frequency corresponding to the pole: $f_0 = \omega_0/2\pi$. The large difference is observed in the values of the "quality factor" Q for real and ideal converters, given in Tables 1 and 2. Similar differences may be observed for control-to-output transmittance H_d, output impedance Z_{out} and input admittance Y_{in}.

$$Y_{\text{in}} = \left.\frac{I_g}{V_g}\right|_{\theta=0} = \frac{D_A^2}{Z_M + B^2 \cdot Z_C}, \tag{13}$$

$$Z_{\text{out}} = \left.\frac{V_o}{I_o}\right|_{V_g=0,\theta=0} = \frac{Z_M \cdot Z_C}{Z_M + B^2 \cdot Z_C}. \tag{14}$$

The frequency dependence and poles and zeros of the above transmittances may be obtained after substitution expressions (4) and (5) for Z_C and Z_M into Eqs. (11)–(14). The resulting expressions for the transmittances may be presented in the form:

$$H_g = H_g(0) \cdot \frac{s/\omega_{Z1} + 1}{T_r\,(s)}, \tag{15}$$

$$H_d = H_d(0) \cdot \frac{(s/\omega_{Z1} + 1) \cdot (s/\omega_{Z2} + 1)}{T_r\,(s)}, \tag{16}$$

$$Z_{\text{out}} = Z_{\text{out}}(0) \cdot \frac{(s/\omega_{Z1} + 1) \cdot (s/\omega_{Z3} + 1)}{T_r(s)}, \tag{17}$$

$$Y_{\text{in}} = Y_{\text{in}}(0) \cdot \frac{s/\omega_{Z4} + 1}{T_r(s)}. \tag{18}$$

The values of transmittances at the frequency equal to zero are:

$$H_g(0) = \frac{D_A \cdot B}{B^2 + R_M \cdot G}, \tag{19}$$

$$H_d(0) = \frac{V_W \cdot B - \dfrac{I_L}{n} \cdot R_M}{B^2 + R_M \cdot G}, \tag{20}$$

$$Z_{\text{out}}(0) = \frac{R_M}{B^2 + R_M \cdot G}, \tag{21}$$

$$Y_{\text{in}}(0) = \frac{D_A^2 \cdot G}{B^2 + R_M \cdot G}. \tag{22}$$

The denominator of the all expressions for transmittances is:

$$T_r\,(s) = \left(\frac{s}{\omega_0}\right)^2 + \frac{s}{Q \cdot \omega_0} + 1, \tag{23}$$

where the angular frequency of the double pole ω_0 and the "quality factor" Q are as follows:

$$\omega_0 = \sqrt{\frac{B^2 + G \cdot R_M}{L \cdot C_Z}}, \tag{24}$$

$$Q = \frac{\sqrt{L \cdot C_Z \cdot \left(B^2 + G \cdot R_M\right)}}{R_M \cdot C_Z + G \cdot L + B^2 \cdot C \cdot R_C}. \tag{25}$$

Other angular frequencies in the expressions for the transmittances are:

$$\omega_{Z1} = \frac{1}{C \cdot R_C}, \tag{26}$$

$$\omega_{Z2} = \frac{I_L \cdot R_M - B \cdot V_W \cdot n}{I_L \cdot L}, \tag{27}$$

$$\omega_{Z3} = \frac{R_M}{L}, \tag{28}$$

$$\omega_{Z4} = \frac{G}{C_Z}. \tag{29}$$

In the theoretical case of ideal converters (without parasitic resistances) one obtains:

$$H_{gi}(0) = \frac{n \cdot D_A}{1 - D_A}, \tag{30}$$

$$H_{di}(0) = \frac{n \cdot V_G}{(1 - D_A)^2}, \tag{31}$$

$$Z_{\text{out}i}(0) = 0, \tag{32}$$

$$Y_{\text{in}i}(0) = \frac{D_A^2 \cdot G}{B^2}, \tag{33}$$

$$\omega_{0i} = \frac{1 - D_A}{n \cdot \sqrt{L \cdot C}}, \tag{34}$$

$$Q_i = B \cdot R \cdot \sqrt{C/L}, \tag{35}$$

$$\frac{1}{\omega_{Z1i}} = \frac{1}{\omega_{Z3i}} = 0, \tag{36}$$

$$\omega_{Z2i} = \frac{-B \cdot V_W \cdot n}{I_L \cdot L}, \tag{37}$$

$$\omega_{Z4i} = \omega_{Z4}. \tag{38}$$

4. Calculations and measurements

From the equations presented in the previous section, the dependencies of the magnitude and phase of the transmittances H_g, H_d, Z_{out} and Y_{in} on frequency may be calculated. The calculations and measurements have been performed for the laboratory model of flyback converter with the following set of parameters: $V_G = 20$ V, $R = 3\ \Omega$, $D_A = 0.5$, and components: transistor TPH3206LDGB with $R_T = 170\ \text{m}\Omega$, diode MBRD 1035 with $R_D = 200\ \text{m}\Omega$, transformer Coilcraft C1174-AL, with $n = 0.2$, $R_{L1} = 0.5\ \Omega$, $R_{L2} = 23\ \text{m}\Omega$, capacitor with $C = 470\ \mu\text{F}$ and $R_C = 76\ \text{m}\Omega$. Figure 5 shows the measurement setup.

In the measurements of the converter transmittances, and parasitic resistances of capacitor and transformer, the Omicron Lab Bode 100 Analyzer has been used. The parasitic resistance values of the diode and transistor are obtained by measurements from DC characteristics. The results of the measurements and calculations of the transmittances are presented in Figs. 6–9 and are compared with calculations based on equations presented in paper [8].

The values of parameters in Eqs. (15)–(25), used in the above calculations are given in Table 1. In addition, Table 2 presents the parameters calculated for an ideal converter.

The influence of parasitic resistances on frequency dependence of selected transmittances may be evaluated by comparison of calculations results for several sets of parasitic resistance

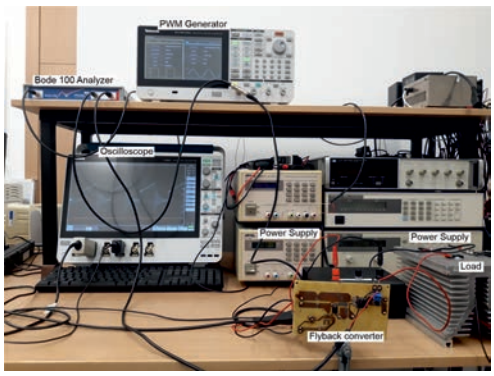

Fig. 5. Measurement setup

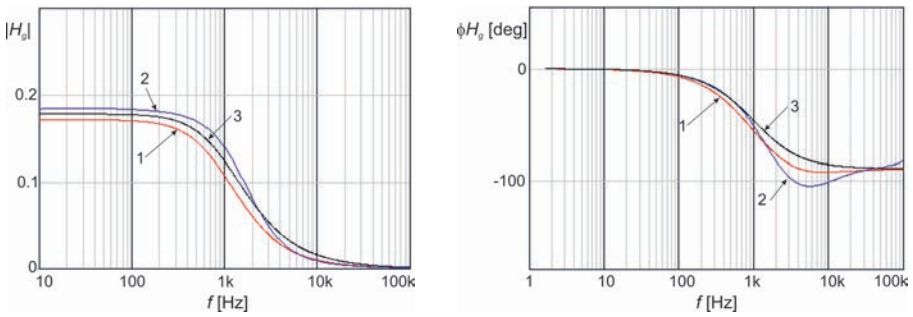

(a) (b)

Fig. 6. Input-to-output transmittance H_g: (a) magnitude; (b) phase. 1) – calculations according to Formula (15); 2) – measurements; 3) – calculations on formulas given in [8]

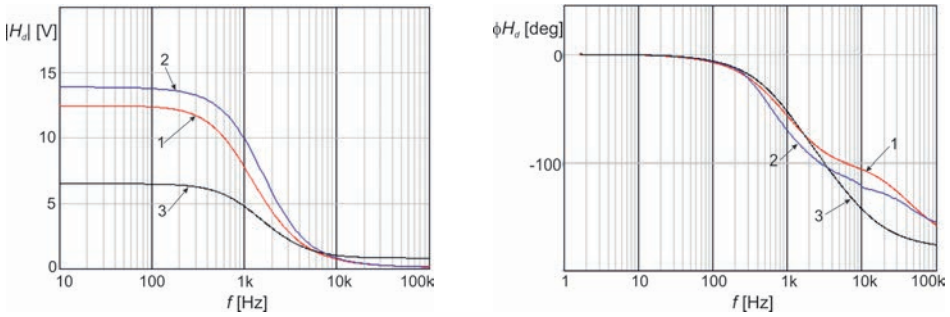

(a) (b)

Fig. 7. Control-to-output transmittance H_d: (a) magnitude; (b) phase. 1) – calculations according to Formula (16); 2) – measurements; 3) – calculations on formulas given in [8]

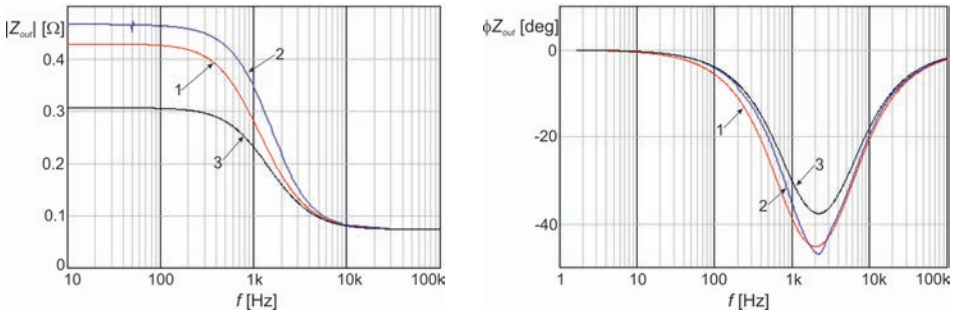

(a) (b)

Fig. 8. Output impedance Z_{out}: (a) magnitude; (b) phase. 1) – calculations according to Formula (17); 2) – measurements; 3) – calculations on formulas given in [8]

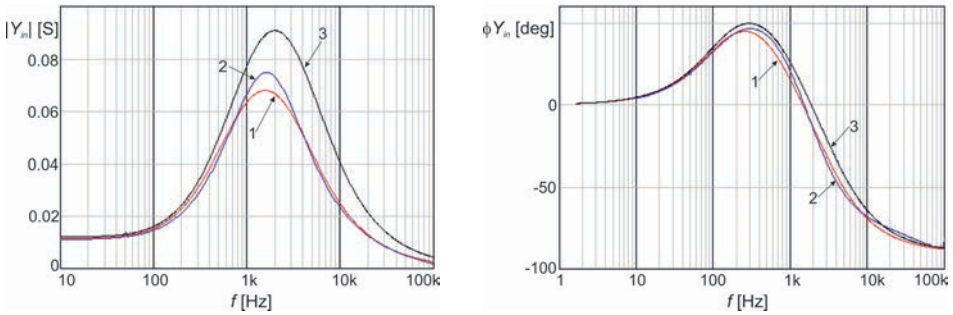

(a) (b)

Fig. 9. Input admittance Y_{in}: (a) magnitude; (b) phase. 1) – calculations according to Formula (18); 2) – measurements; 3) – calculations on formulas given in [8]

Table 1. The parameter values of the transfer function of the converter with parasitic elements, calculated using Formulas (15)–(22) and (24)–(29)

Symbol	**Value**	**Unit**
H_g (0)	0.171	[V/V]
H_d (0)	12.464	[V]
$Z_{\text{out}}(0)$	0.428	[Ω]
$Y_{\text{in}}(0)$	0.011	[S]
ω_0	$9.911 \cdot 10^3$	[rad/s]

Table 1 continued on next page

Table 1 continued from previous page

Symbol	Value	Unit
Q	0.414	
$\omega_{Z\,1}$	$2.8 \cdot 10^4$	[rad/s]
$\omega_{Z\,2}$	$-2.611 \cdot 10^5$	[rad/s]
$\omega_{Z\,3}$	$2.027 \cdot 10^4$	[rad/s]
$\omega_{Z\,4}$	691.697	[rad/s]

Table 2. Parameter values of the transfer functions of the ideal converter, calculated from Formulas (30)–(38)

Symbol	Value	Unit
H_{gi} (0)	0.2	[V/V]
H_{di} (0)	16	[V]
$Z_{\mathrm{out}i}(0)$	0	[Ω]
$Y_{\mathrm{in}i}(0)$	0.013	[S]
ω_{0i}	$9.292 \cdot 10^3$	[rad/s]
Q_i	13.102	
$\omega_{Z\,2i}$	$-2.813 \cdot 10^5$	[rad/s]
ω_{Z4i}	691.697	[rad/s]

values. The examples of such comparisons for the output impedance of converter is shown in Figs. 10 and 11. Graphs in Fig. 10 are obtained for several values of parasitic resistances of transistor (R_T) and diode (R_D) assumed to be equal ($R_T = R_D$), with other parasitic resistance values the same as used in calculations presented in Figs. 6–9. According to calculations presented in Fig. 11, the influence of resistances R_T and R_D on the output impedance differs substantially. It may be explained by the form of Eq. (6) for equivalent resistance R_M in which the resistance R_{DL}, dependent mainly on the diode resistance R_D, is divided by n^2. In the converter under considerations, the parameter n equals 0.2 therefore, according to Eqn. (6), the term connected with the resistance R_D is multiplied by 25.

Another comparison is presented in Fig. 12 and concerns the input-to-output transmittance H_g. The curves for the real converter (with parasitic resistances) are compared with curves for the ideal converter (with all parasitic resistances set to zero). The substantial differences are observed, especially in the vicinity of the frequency corresponding to the pole: $f_0 = \omega_0/2\pi$. The large difference is observed in the values of the "quality factor" Q for real and ideal converters, given in Tables 1 and 2. Similar differences may be observed for control-to-output transmittance H_d, output impedance Z_{out} and input admittance Y_{in}.

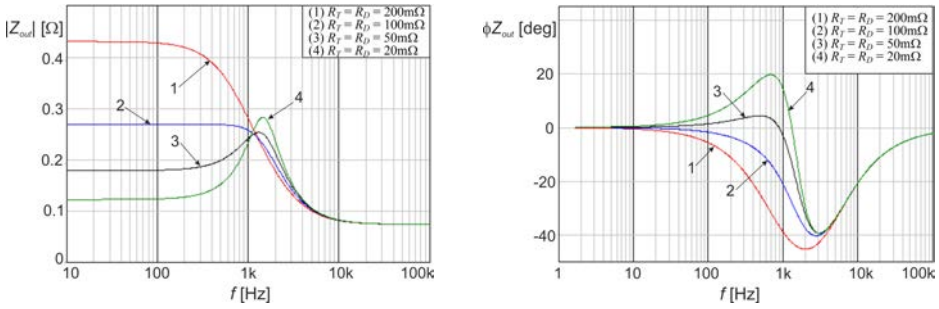

(a) (b)

Fig. 10. The magnitude (a) and phase (b) of the output impedance of converter calculated for several values of the parasitic resistances of transistor R_T and diode R_D.

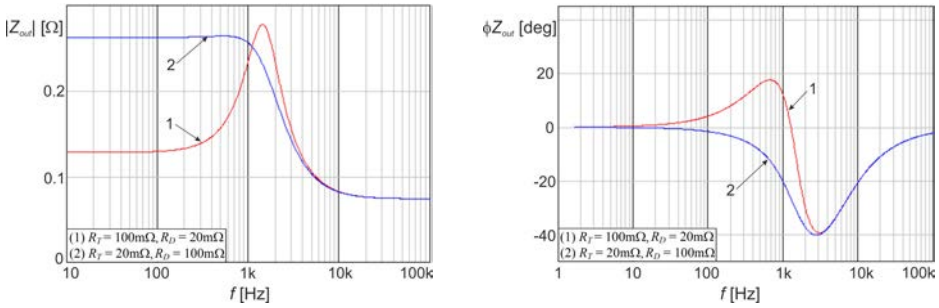

(a) (b)

Fig. 11. The magnitude (a) and phase (b) of the output impedance of converter calculated for several values of the parasitic resistances of transistor R_T and diode R_D.

5. Discussion of the obtained results

The theoretical averaged models represented by Figs. 3 and 4 and Eqs. (15)–(25), include parasitic resistances of circuit components R_T, R_D, R_{L1}, R_{L2} and R_C, and are more accurate than ideal models (without parasitic resistances) but are still approximate, because the nonlinearities of components are neglected, and the process of averaging itself introduces some inaccuracies. In addition, the measurements of component parameters introduce some errors. As a result, the consistency of the results of measurements and calculations presented in Figs. 6–9 may be appraised as very good.

The influence of parasitic resistances on converter transmittances has been evaluated by comparison of transmittance characteristics calculated for different sets of these resistances. The most spectacular seems to be the comparison of the input-to-output transmittance characteristics for ideal and real converter shown in Fig. 12, where the magnitude of H_g at the resonant frequency $f_0 = \omega_0/2\pi$ calculated for ideal case is many times greater than for real converter with parasitic

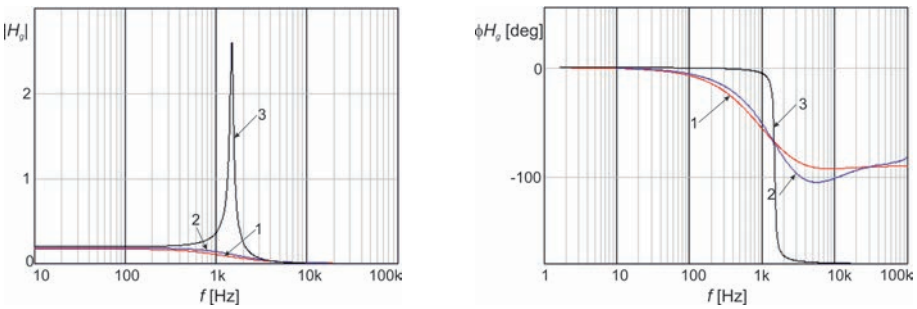

(a) (b)

Fig. 12. Comparison of the input-to-output transmittance H_g for real converter and ideal converter: (a) magnitude; (b) phase. 1) – calculations with parasitic resistances included; 2) – measurements; 3) – calculations for ideal converter

resistances. Very similar relations are obtained for other transmittances (not shown in this paper). Therefore, the design of the control circuit of converter based on the ideal description of the power stage seems to be useless.

The results of the present paper are compared with the results of paper [8], where the parasitic resistance of components is also taken into account. The methods of the obtaining the formulas for transmittances are different, because are based on different ways of the averaged models derivation. In our paper it is separation of variables approach, and in [8] it is switch averaging technique. As a result, the final expressions for transmittances in [8] and in the present paper are different. The formulas describing the transmittances in our work seems to be simpler than in [8]. Results of our calculations are compared with the results of paper [8] in Figs. (6)–(9). The shape of the corresponding curves is practically the same but the numerical values of the magnitude of control-to-output transmittance and output impedance differs substantially. The consistency of the calculation results based on our theoretical formulas with measurements is better than that in the case of formulas presented in [8]. However, it should be pointed out, that the comparisons cannot be performed exactly, because the parasitic resistances in our paper and in [8] are described differently. The similar set of transmittances is presented in the paper [11] where only the ideal converter is considered and no numerical results of calculations are shown, so the quantitative comparison of numerical with that in our work is not performed.

6. Summary

The object of the paper are small-signal transmittances of the power stage of flyback DC–DC converter working in the continuous conduction mode. The mathematical formulas for transmittances are derived from the large signal averaged model of converter, obtained with the separation of variables approach. The parasitic resistances of all the converter components are included in the derivation of transmittances. The formulas for several small-signal parameters, in particular the angular frequencies corresponding to poles and zeros of the frequency

dependence of transmittances are found. The laboratory model of converter has been built and the frequency dependencies of the magnitude and phase of the transmittances have been measured. The measurement results are compared with the results of the numerical calculations based on theoretical formulas. The good consistency of the results of the calculations and measurements is observed, therefore the correctness of the formulas for transmittances is confirmed. The influence of the parasitic resistance values on the small-signal transmittances of converter is studied and, in particular, the substantial differences in the frequency characteristics between the real and ideal converter are shown. It means, that the neglecting the parasitic resistances of the converter components in the description of the power stage may lead to serious errors in the design procedure of the control subcircuit.

The results of the calculations based on our formulas for small-signal transmittances are compared with the calculations based on formulas presented in [8]. The shape of the frequency dependencies of the transmittances for both cases is similar but the numerical values of the magnitude of the control-to-output transmittance and output impedance differ, especially in the low frequency range and the consistency of our calculations with the experiments is better.

The knowledge of the frequency dependence of the DC–DC converter small signal transmittances is crucial in the design process of the control circuit for converter. The transmittances for the flyback converters, that are presented in the paper, have a convenient form and are experimentally verified therefore, the results of the paper may assure the improvement of the process of flyback converter control circuits design.

References

[1] Erickson R.W., Maksimovic D., *Fundamentals of Power Electronics*, 3-rd Edition, Springer (2020), DOI: 10.1007/978-3-030-43881-4.

[2] Kazimierczuk M.K., *Pulse-Width Modulated DC–DC Power Converters*, J. Wiley (2008), DOI: 10.1002/9780470694640.

[3] Milanovič M. *et al*., *Reduction of Ringing Losses in Flyback Converter by Using the RC–RCD Clamp Circuit*, Automatika 47, no. 1–2, pp. 31–37 (2006).

[4] Pandey S.K., Patti S.L., Rajguru V.S., *Isolated Flyback Converter, Designing, Modeling and Suitable Control Strategies*, Int. Conf. on Advances in Power Electronics and Instrumentation Engineering (2014), DOI: 02.PEIE.2014.5.15.

[5] Jayalaksami N.S., Gaonkar D.N., Naik A., *Design and Analysis of Dual Output Flyback Converter for Standalone PV/Battery System*, International Journal of Renewable Energy Research, vol. 7, no. 3, pp. 1032–1040 (2017), DOI: 10.20508/ijrer.v7i3.5825.g7134.

[6] Janke W., *Averaged Models of Pulse-Modulated DC–DC Converters*,

Part II. Models Based on the Separation of Variables, Archives of Electrical Engineering, vol. 61, no. 4, pp. 633–654 (2012), DOI: 10.2478/v10171-012-0046-7.

[7] Janke W., *Equivalent Circuits for Averaged Description of DC–DC Switch-Mode Power Converters Based on Separation of Variables Approach*, Bull. of the Polish Academy of Sciences, vol. 61, no. 3, pp. 711–723 (2013), DOI: 10.2478/bpasts-2013-0076.

[8] Kazimierczuk M.K., Nguyen S.T., *Small-Signal Analysis of Open-Loop PWM Flyback DC–DC Converter for CCM*, Proc. of the IEEE National Aerospace and Electronic Conference (1995), DOI: 10.1109/NAECON.1995.521914.

[9] Rushil K.K., *AC Modeling of Power Stage in Flyback Converter*, Appl. Report SLVA589, Texas Instruments (2013).

[10] Akbarabadi S.A., Atighechi H., Jatskevich J., *Circuit-Averaged and State-Space-Averaged-Value Modeling of Second-Order Flyback Converter in CCM and DCM Including Conduction Losses*, 4^{th} International Conference on Power Engineering, Energy and Electrical Drives, Istanbul, Turkey, pp. 995–1000 (2013), DOI: 10.1109/PowerEng.2013.6635746.

[11] Vu T.T., *Non-linear Dynamic Transformer Modelling and Optimum Control Design of Switched-mode Power Supplies*, PhD Thesis, National University of Ireland Maynooth (2014).

[12] Raj A.S., Siddeshwar A.M., Guruswamy K.P., Maheshan C.M., Sanekere V.C., *Modelling of flyback converter using state space averaging technique*, Computing and Communication Technologies (CONECCT), IEEE International Conference on Electronics (2015), DOI: 10.1109/CONECCT.2015.7383871.

[13] Xu S. *et al*., *An accurate Small Signal Modeling and Control Loop Design of Active Clamp Flyback Converter*, 10^{th} International Conference of Power Electronics-ECCE Asia (2019), DOI: 10.23919/ICPE2019-ECCEAsia42246.2019.8797022.

[14] Kleebchampee W., Bunlaksananusorn C., *Modeling and Control Design of a Current-Mode Controlled Flyback Converter with Optocoupler Feedback*, Power Electronics and Drives Systems, pp. 787–792 (2005), DOI: 10.1109/PEDS.2005.1619792.

[15] Vu T.T., O'Driscoll S., Ringwood J.V., *Primary-Side Sensing for a Flyback Converter in Both Continuous and Discontinuous Conduction Mode*, ISSC, NUI, Maynoth (2012), DOI: 10.1049/ic.2012.0195.

[16] Fa-Quiang W., Xi-Kui M., *Effects of Switching Frequency and Leakage Inductance on Slow-Scale Stability in a Voltage Controlled Flyback Converter*, Chin. Phys. B, vol. 22, no. 12, pp. 120504-1–120504-8 (2013), DOI: 10.1088/1674-1056/22/12/120504.

[17] Chen S.Y., *Small-Signal Model for a Flyback Converter with Peak Current Mode Control*, IET Power Electronics, vol. 7, iss. 4, pp. 805–810 (2014), DOI: 10.1049/iet-pel.2013.0326.

[18] Kasundra N., Kumar A., *Design and Simulation of Flyback Converter in MATLAB using PID Controller*, International Journal of Advanced Research in Electrical, Electronics and Instrumentation Engineering, vol. 5, no. 2, pp. 960–965 (2016), DOI: 10.15662/IJAREEIE.2016.0502057.

[19] Cheng C.H., Chen C.J., Wang S.S., *Small-Signal Model of Flyback Converter in Continuous-Conduction Mode with Peak-Current Control at Variable Swiching Frequency*, IEEE Trans. on Power Electronics, vol. 33, iss. 5, pp. 4125–4156 (2018), DOI: 10.1109/TPEL.2017.2716830.

[20] Kazimierczuk M.K., Saini D.K., Ayachit A., *Averaged Current-Mode Control of DC–DC Power Converters*, J. Wiley & Sons (2022).

[21] Saini D.K., Kazimierczuk M.K., *Open-loop transfer functions of buck-boost converter by circuit-averaging techniques*, IET Power Electronics, vol. 12, no. 11, pp. 2858–2864 (2019), DOI: 10.1049/iet-pel.2018.5514.

[22] Janke W., Bączek M., Kraśniewski J., *Large-Signal Averaged Models of the Non-ideal Flyback Converter Derived by the Separation of Variables*, Bulletin of the Polish Academy of Sciences: Technical Sciences, vol. 68, no. 1, pp. 81–88 (2020), DOI: 10.24425/bpasts.2020.131838.

[23] Janke W., Bączek M., Kraśniewski J., *Input characteristics of a non-ideal DC–DC flyback converter*, Bulletin of the Polish Academy of Sciences: Technical Sciences, vol. 67, no. 5, pp. 841–849 (2019), DOI: 10.24425/bpasts.2019.130884.